Electronic Supplementary Information

A general strategy for embedding ultrasmall CoM_x nanocrystals (M = S, O, Se, and Te) in hierarchical porous carbon nanofibers for high-performance potassium storage

Chenling Lai, Zhuangzhaung Zhang, Yifan Xu, Jiaying Liao, Zhenhua Xu, Zuyue Yi, Jingyi Xu, Jianchun Bao and Xiaosi Zhou**

Jiangsu Key Laboratory of New Power Batteries, Jiangsu Collaborative Innovation Center of Biomedical Functional Materials, School of Chemistry and Materials Science, Nanjing Normal University, Nanjing, 210023, China

*Corresponding authors.

E-mail: baojianchun@njnu.edu.cn; zhouxiaosi@njnu.edu.cn

Experimental Section

Synthesis of ZIF-67 nanocrystals. In a typical synthesis, 3.64 g $Co(NO_3)_2 \cdot 6H_2O$ was dissolved in 125 mL *N*, *N*-Dimethylformamide (DMF) to form solution A. 8.2 g 2-methylimidazole was dissolved in another 125 mL DMF to produce solution B. Subsequently, solution B was added into solution A quickly and then the mixture was magnetically stirred for 2 h at ambient temperature. After the reaction, the product was harvested and washed with DMF.

Synthesis of ZIF-67/PAN nanofibers. The as-collected ZIF-67 nanocrystals (0.5 g) were redispersed in 10 mL DMF by sonication to generate a uniform suspension. Afterwards, 0.7 g polyacrylonitrile (PAN) was added to the resulting ZIF-67/DMF dispersion solution and was then dissolved completely by vigorous stirring for 12 h at 60 °C. Then, the resultant homogeneous purple solution was loaded into a 10 mL plastic syringe connected with a 21-gauge blunt tip needle. The flow rate of the solution was controlled to be 0.3 mL h^{-1} by a syringe pump. A 15 kV high voltage was applied between the needle and the aluminum foil to initiate electrospinning. The aluminum foil was grounded and utilized to collect the nanofibers, and the distance between the needle and the nanofiber collector was fixed at 12 cm. After electrospinning, the ZIF-67/PAN nanofibers were achieved.

Synthesis of ultrasmall Co nanoparticles-embedded in hierarchically porous carbon nanofibers (u-Co@HCFs): In a typical synthesis, the as-collected non-woven ZIF-67/PAN nanofiber film was carbonized in a tube furnace at 625 °C for 0.5 h with a heating rate of 1°C min^{-1} under a H_2/Ar (5/95v/v) flow to obtain u-Co@HCFs.

Synthesis of ultrafine CoS_2 nanoparticles-impregnated in hierarchically porous carbon nanofibers (u-CoS_2@HCFs): Typically, the as-synthesized u-Co@HCFs were placed in a porcelain boat. The boat was heated in a tube furnace at 400 °C for 1 h at a heating rate of 5 °C min^{-1} under a H_2S/Ar (5/95 v/v) flow. After the temperature was naturally cooled down to ambient temperature, the product of u-CoS_2@HCFs was gathered for further tests.

Synthesis of ultrafine Co_3O_4 nanoparticles-encapsulated in hierarchically porous carbon nanofibers (u-Co_3O_4@HCFs): In a typical procedure, the as-formed u-Co@HCFs were put into a

porcelain boat. The boat was heated at 360 °C in a muffle furnace under an air environment for 5 min with a temperature ramp of 5 °C min^{-1}. After the temperature naturally drops to room temperature, the product of u-Co_3O_4@HCFs was collected for further measurements.

Synthesis of ultrafine CoSe nanoparticles-infiltrated in hierarchically porous carbon nanofibers (u-CoSe@HCFs): Typically, the as-obtained u-Co@HCFs (0.2 g) was mixed with selenium power (0.2 g), and then the resulting mixture was placed in a porcelain boat. The boat was heated in a tube furnace at 350 °C for 3 h with a warming rate of 2 °C min^{-1} under flowing H_2/Ar (5/95 v/v) atmosphere. After cooling down naturally, the product of u-CoSe@HCFs was gathered for further tests.

Synthesis of ultrafine CoTe nanoparticles-embedded in hierarchically porous carbon nanofibers (u-CoTe@HCFs): In a typical synthesis, the as-fabricated u-Co@HCFs (0.2 g) was mixed with tellurium power (0.2 g), and then the obtained mixture was put into a porcelain boat. The boat was heated at 450 °C for 2 h with a temperature ramp of 5 °C min^{-1} under a H_2/Ar (5/95 v/v) flow. After the temperature was naturally cooled down to room temperature, the product of u-CoTe@HCFs was achieved for further measurements.

Synthesis of hierarchically porous carbon nanofibers (HCFs): Typically, the as-produced u-Co@HCFs (0.2 g) was first mixed with 20 mL HCl aqueous solution (2 M) by vigorous stirring for 6 h at room temperature. Then the resulting mixture was transferred into a sealed Teflon-lined stainless-steel autoclave and held at 100 °C for 6 h. Finally, the product of HCFs was collected by centrifugation and washed with water and ethanol and then dried in an oven at 70 °C.

Materials Characterization: The morphologies and microstructures were examined by field-emission scanning electron microscope (FESEM; JSM-7600F) and transmission electron microscope (TEM; JEM-2100F). The crystal structures were determined by X-ray diffraction (XRD; Rigaku, SmartLab). Raman spectra were performed on a HORIBA LabRAM HR Evolution with a 532 nm laser as an excitation source. Nitrogen adsorption/desorption isotherms were recorded using an ASAP 2020 surface area-pore size analyzer. Thermogravimetric analysis (TGA) was measured by using a NETZSCH STA 449 F3 thermogravimetric analyzer in air with a heating rate of 10 °C

min^{-1}. X-ray photoelectron spectroscopy (XPS) spectra were conducted on an EscaLab Xi+ electron spectrometer. The composition was surveyed by energy-dispersive X-ray spectroscope (EDX) attached to FESEM. The elemental contents of synthesized material were investigated by inductively coupled plasma (ICP; Shimadzu, ICPS-8100).

Electrochemical Measurements: The electrochemical characterizations were carried out using CR2032 coin-type batteries. The working electrodes were fabricated by pasting the slurry containing 80 wt% active material, 10 wt% Super-P carbon black, and 10 wt% polyvinylidene fluoride binder onto a copper foil. The loading mass of active material is in the range of 0.8−1.2 mg cm^{-2}. The electrolyte was 1.5 M KFSI in a mixture of ethylene carbonate (EC) and diethyl carbonate (DEC) (1:1 v/v). Potassium thin disks and glass fiber (Whatman) were employed as the counter and reference electrodes and the separators, respectively. All the cells were assembled in an argon-filled glovebox (MBRAUN) with water/oxygen content lower than 0.1 ppm. The galvanostatic discharge/charge tests were conducted with a voltage range of 0.01−3.0 V vs K/K^+ on a Land CT2001A battery testing system. Cyclic voltammetry (CV) measurements were performed on a PARSTAT 4000 electrochemical workstation.

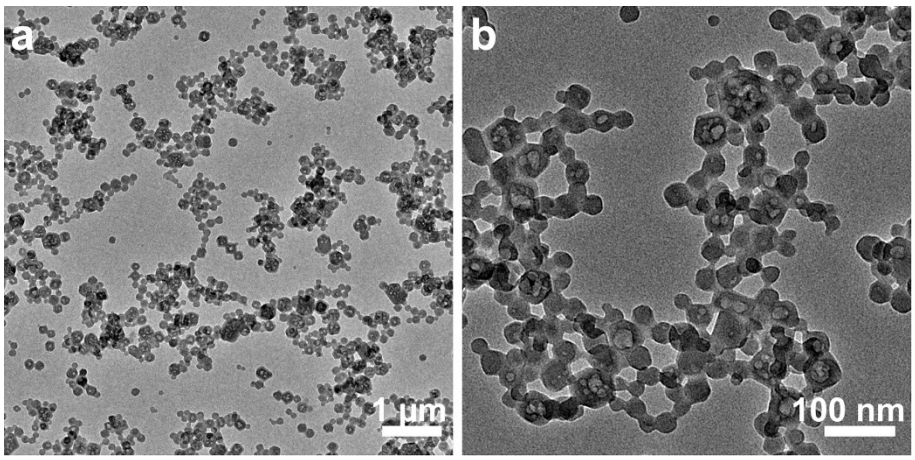

Fig. S1 (a, b) TEM images of ZIF-67 nanoparticles.

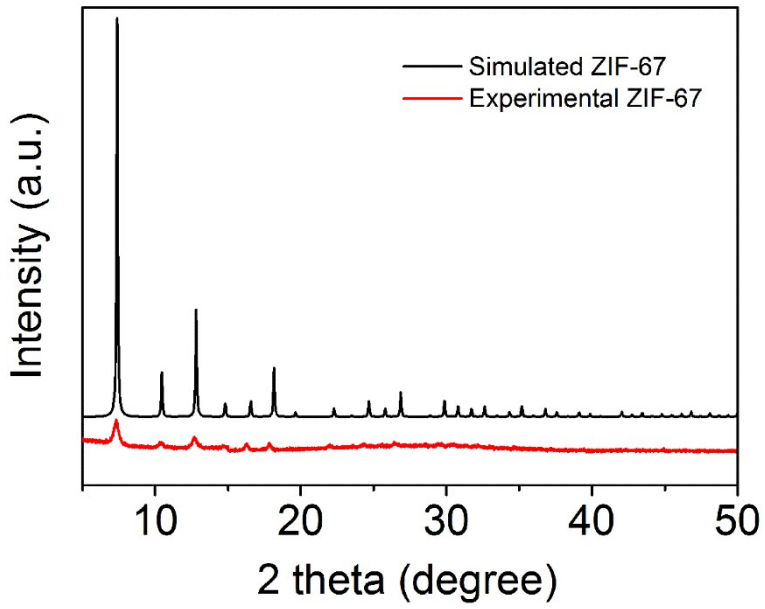

Fig. S2 XRD pattern of the ZIF-67 nanoparticles.

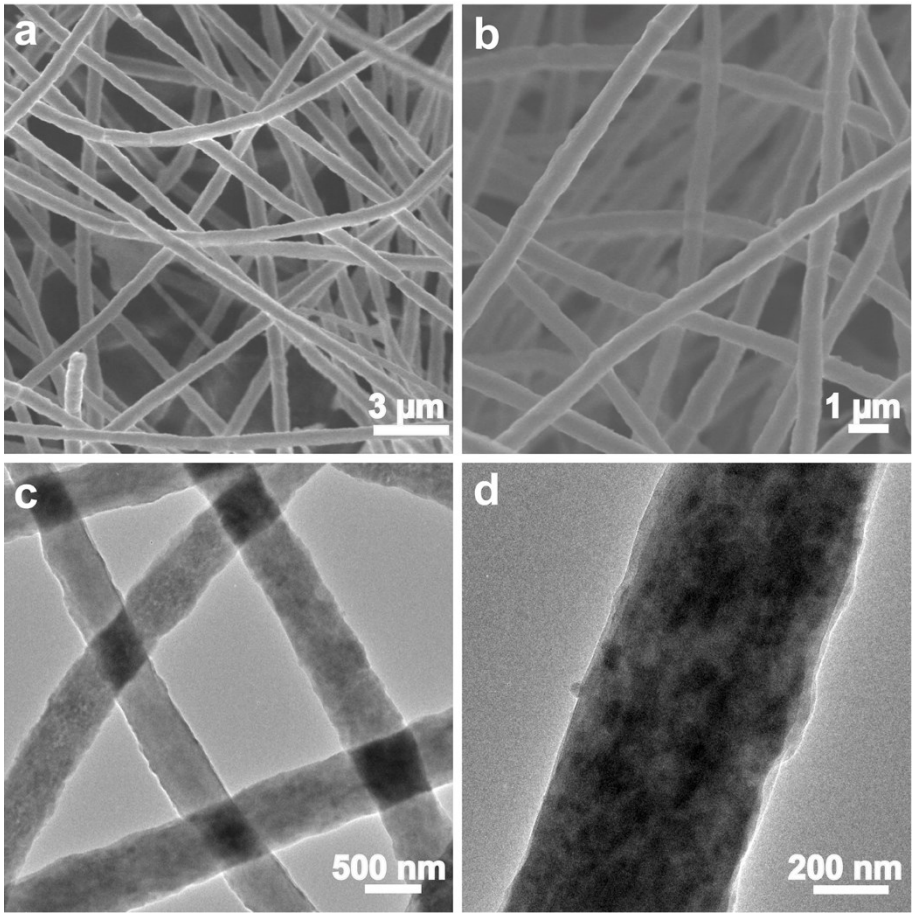

Fig. S3 (a, b) SEM images and (c, d) TEM images of ZIF-67/PAN nanofibers.

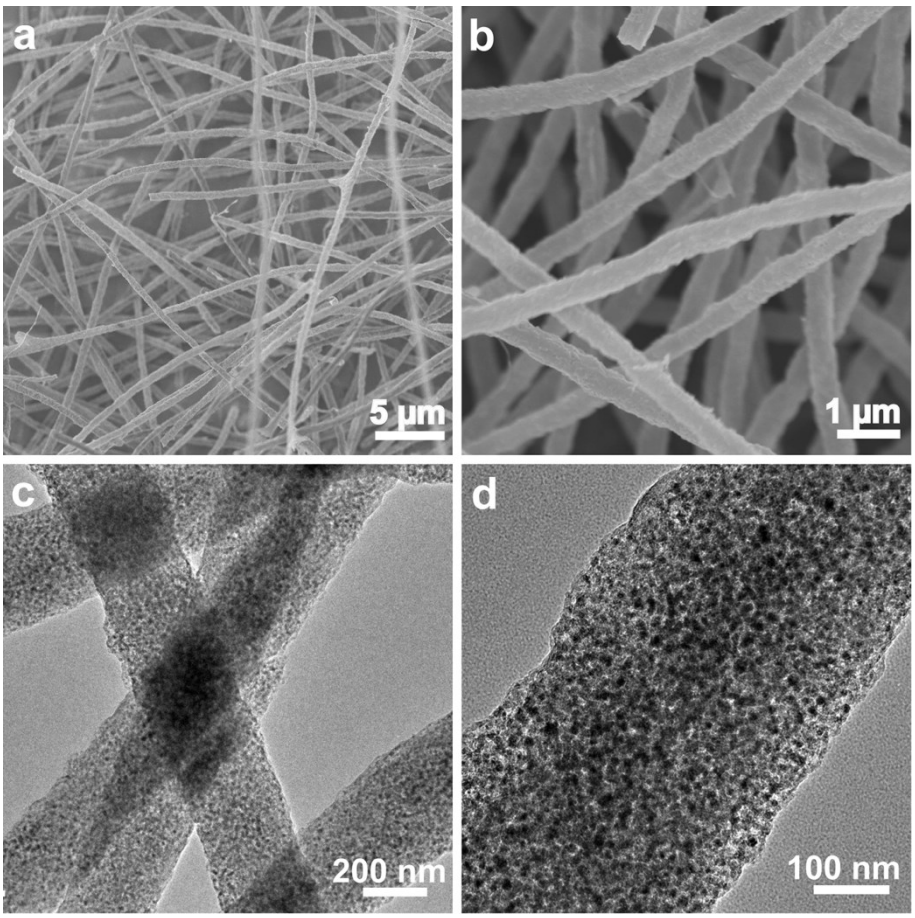

Fig. S4 (a, b) SEM images and (c, d) TEM images of u-Co@HCFs.

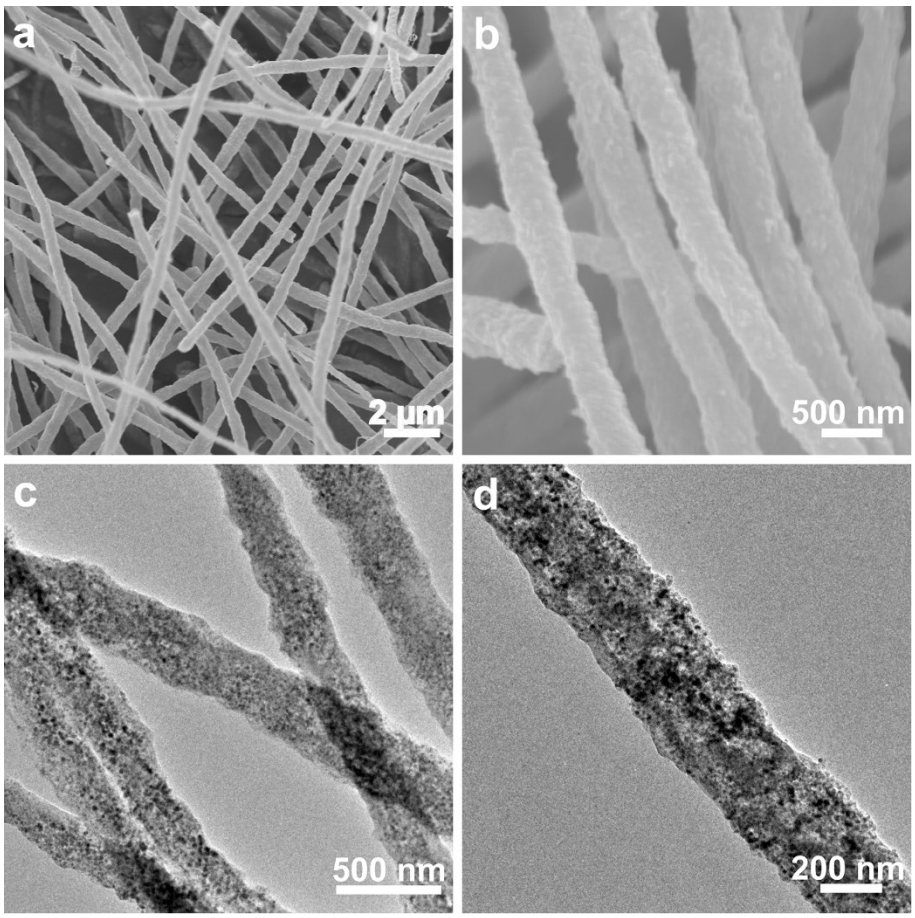

Fig. S5 (a, b) SEM images and (c, d) TEM images of low-density Co ultrafine nanoparticles-embedded in hierarchically porous carbon nanofibers (denoted LD-Co@HCFs).

The preparation of LD-Co@HCFs was the same as that of u-Co@HCFs, except that reducing the amount of ZIF-67 from 0.5 g to 0.4 g when preparing the ZIF-67/DMF dispersion solution.

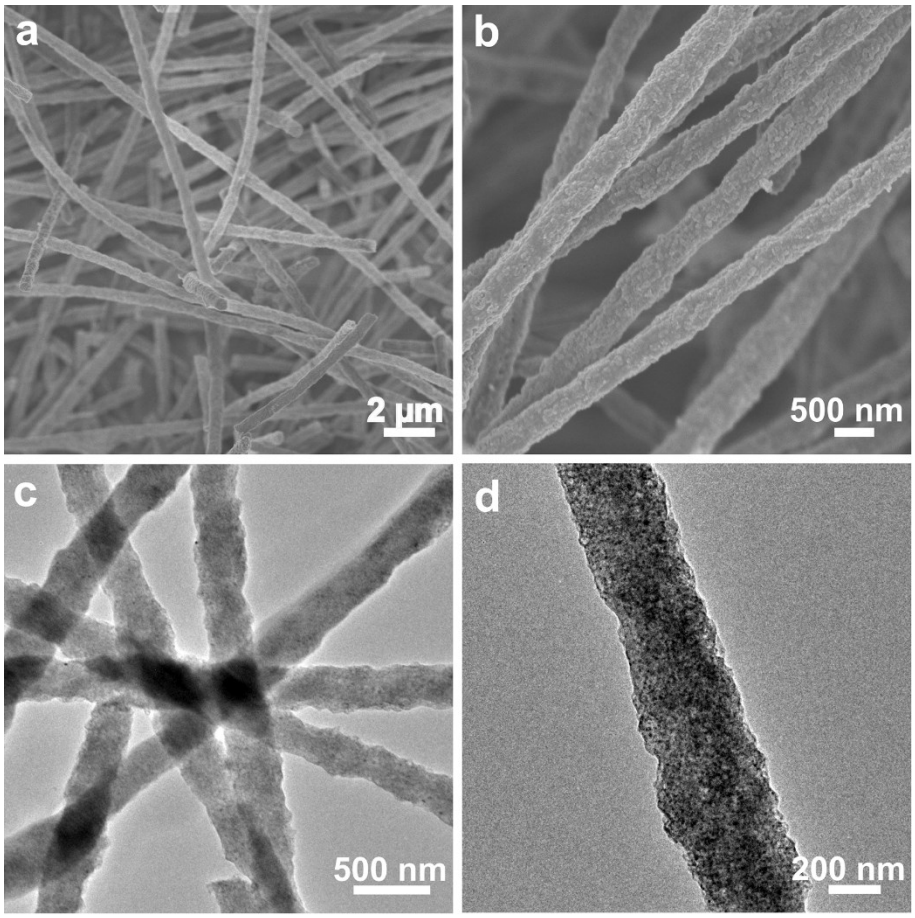

Fig. S6 (a, b) SEM images and (c, d) TEM images of large-size Co nanoparticles-impregnated in hierarchically porous carbon nanofibers (denoted LS-Co@HCFs).

The fabrication of LS-Co@HCFs was the same as that of u-Co@HCFs, except that increasing the amount of ZIF-67 from 0.5 g to 0.6 g when preparing the ZIF-67/DMF dispersion solution.

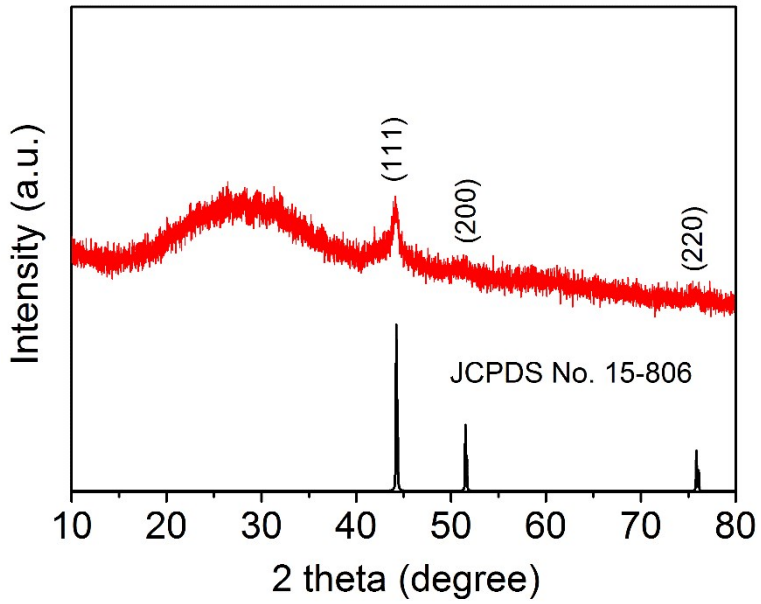

Fig. S7 XRD pattern u-Co@HCFs and standard XRD pattern of cobalt.

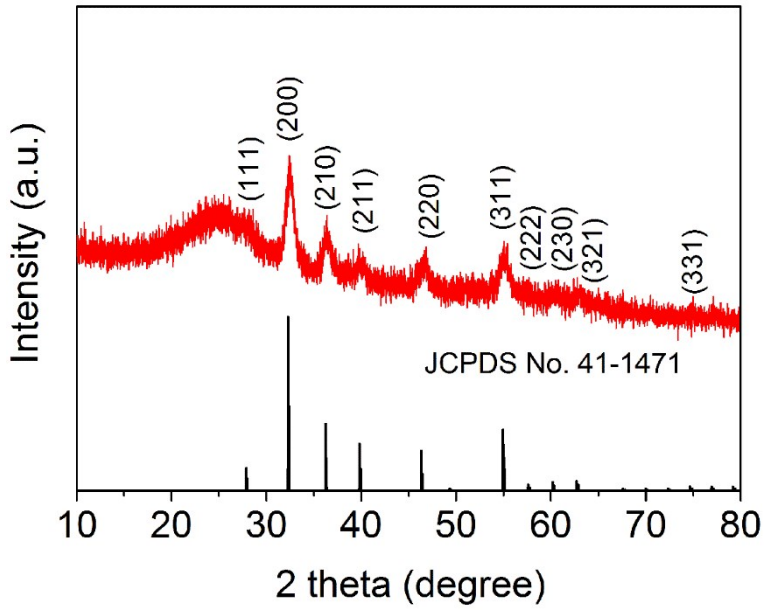

Fig. S8 XRD pattern u-CoS_2@HCFs and standard XRD pattern of cobalt disulfide.

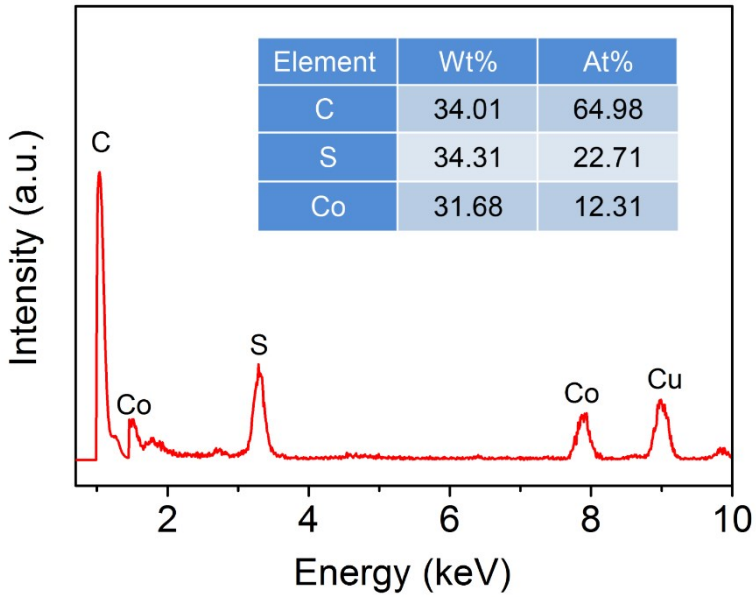

Fig. S9 EDX spectrum of u-CoS_2@HCFs.

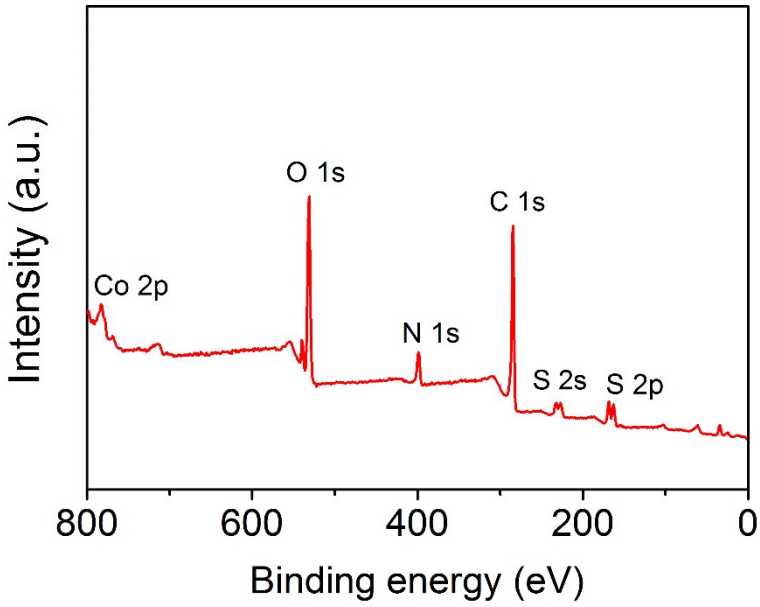

Fig. S10 XPS survey scan of u-CoS_2@HCFs.

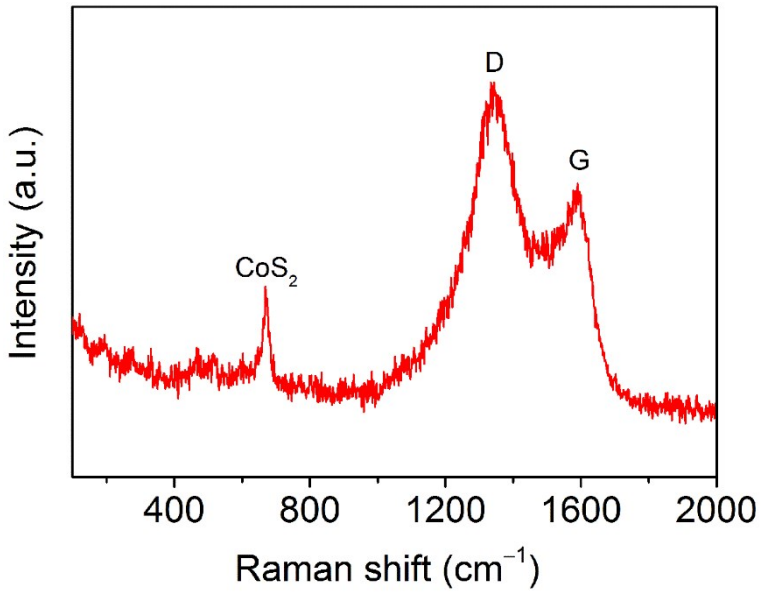

Fig. S11 Raman spectrum of u-CoS_2@HCFs.

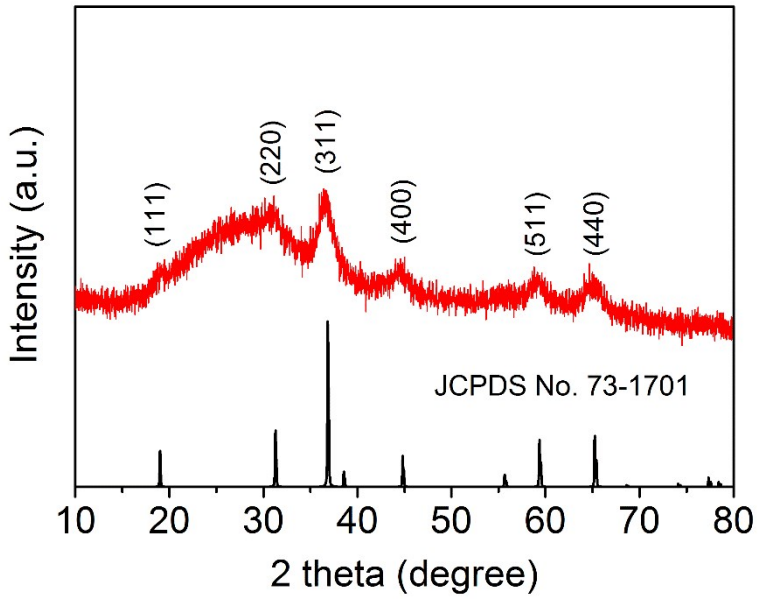

Fig. S12 XRD pattern u-Co_3O_4@HCFs and standard XRD pattern of Co_3O_4.

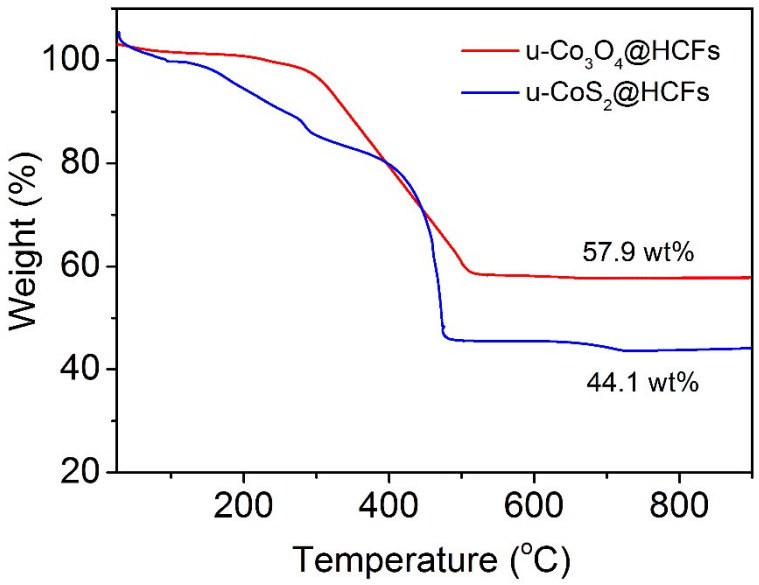

Fig. S13 TGA curves of u-CoS_2@HCFs and u-Co_3O_4@HCFs under an air atmosphere with a temperature ramp of 10 °C min^{-1} from room temperature to 900 °C.

The weight fraction of CoS_2 in u-CoS_2@HCFs can be determined by TGA based on the complete weight loss of HCFs combustion and the partial weight loss from the transformation of CoS_2 into Co_3O_4. According to the equation below, the content of CoS_2 in the nanofibers is calculated to be about 66 wt%.

$$CoS_2\ (wt\%) = \frac{\text{final weight of u-}CoS_2\text{@HCFs}}{\text{initial weight of u-}CoS_2\text{@HCFs}} \times \frac{3 \times \text{molecular weight of } CoS_2}{\text{molecular weight of } Co_3O_4}$$

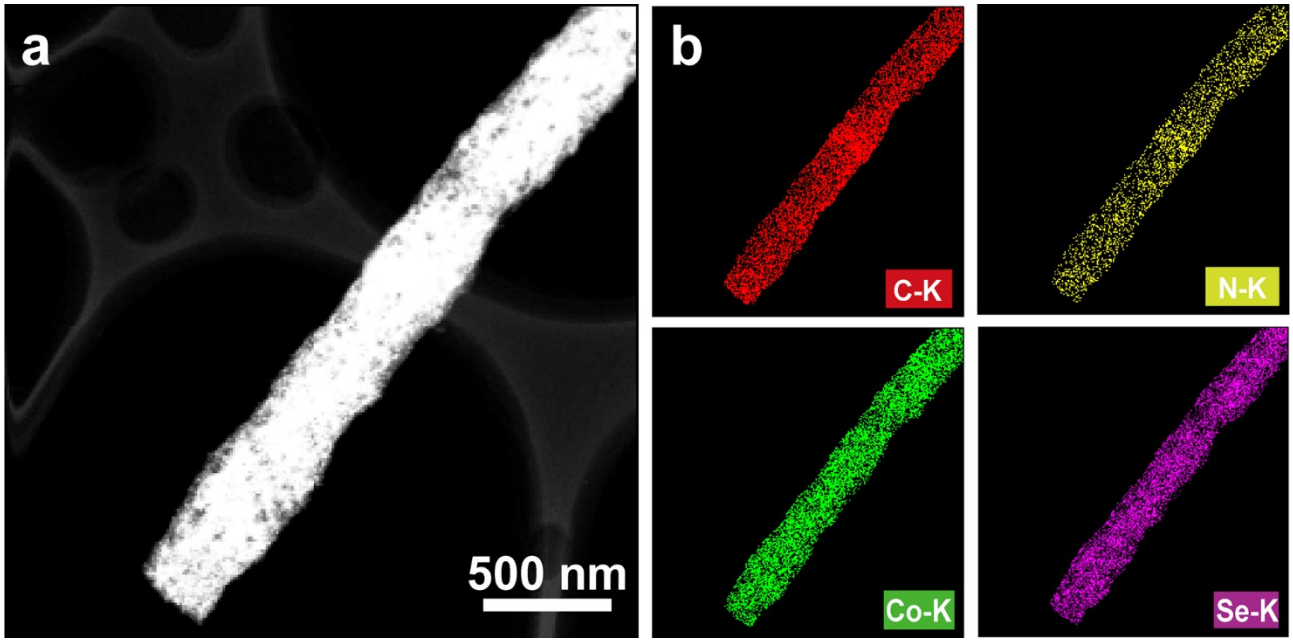

Fig. S14 (a) Scanning transmission electron microscopy (STEM) image and (b) corresponding elemental mapping images of u-CoSe@HCFs.

The EDX measurement on u-CoSe@HCFs illustrates that the homogeneous elemental distribution of C, N, Co, and Se elements within hierarchically porous carbon nanofibers.

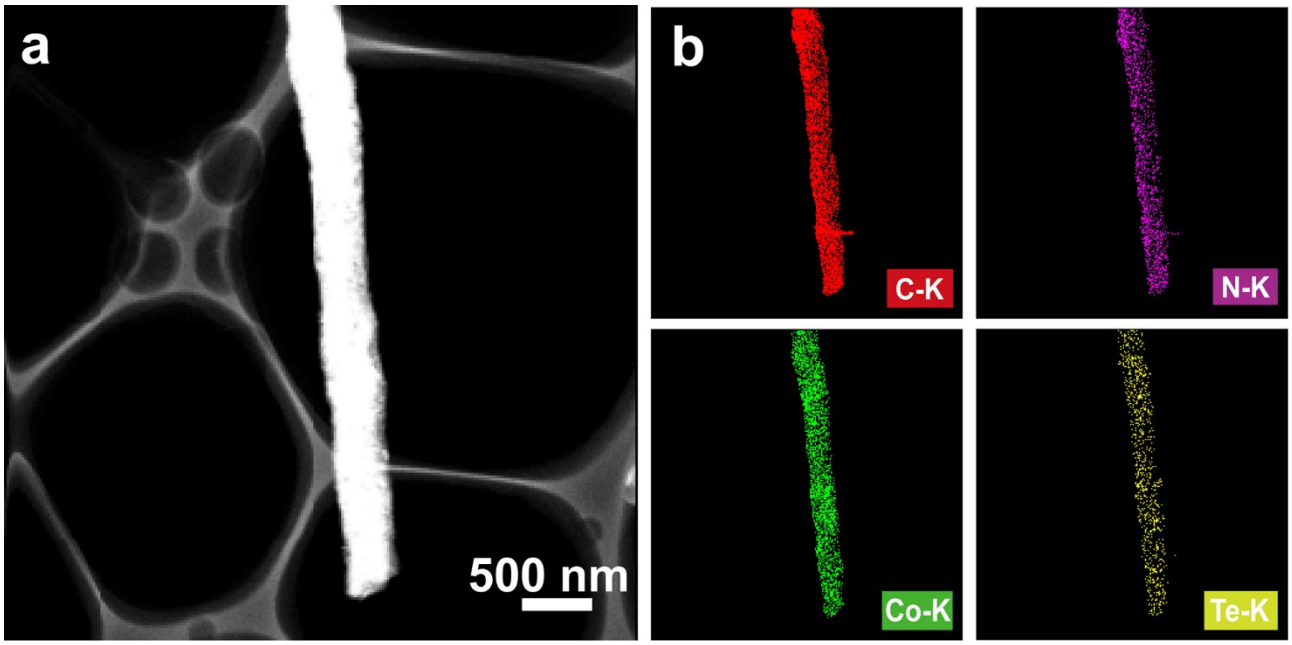

Fig. S15 (a) STEM image and (b) corresponding elemental mapping images of u-CoTe@HCFs.

The EDX investigation on u-CoTe@HCFs displays that the uniform elemental distribution of C, N, Co, and Te elements within hierarchically porous carbon nanofibers.

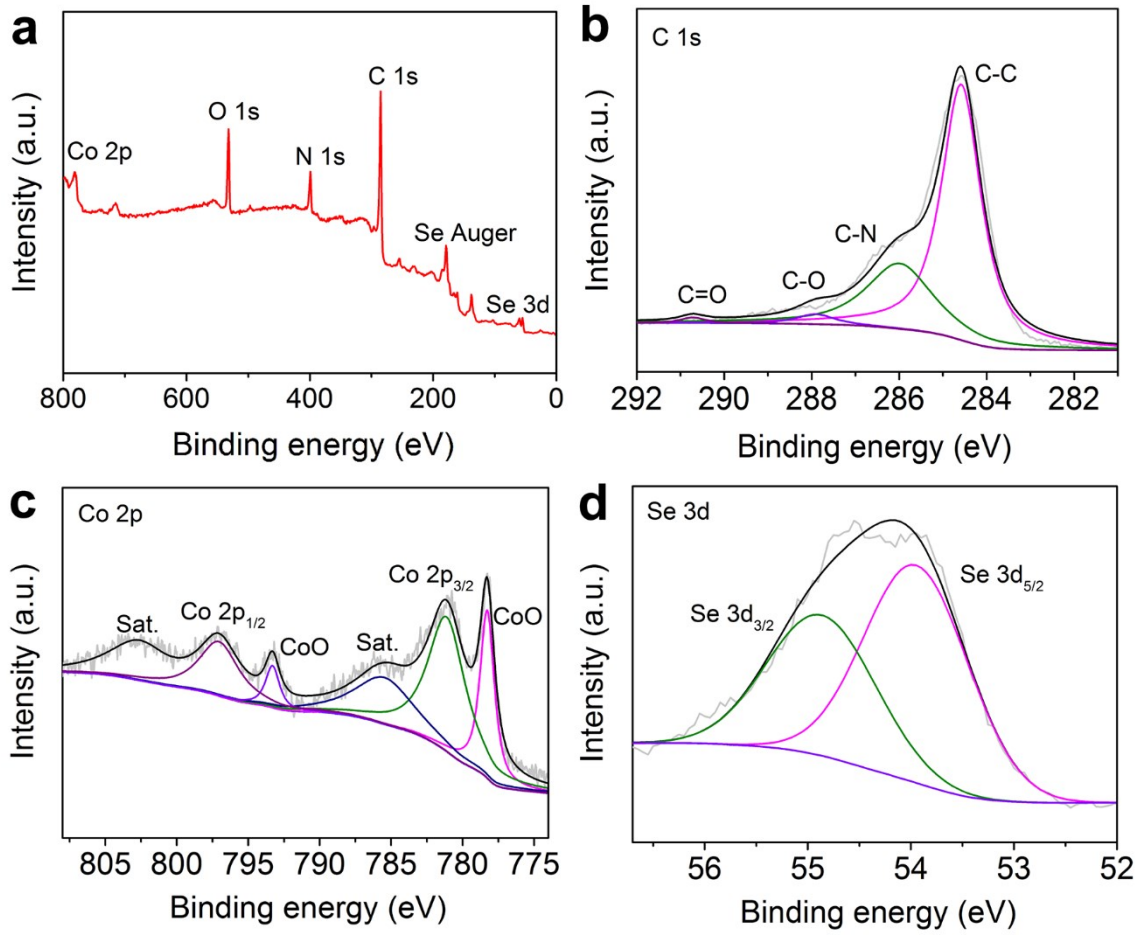

Fig. S16 (a) XPS survey scan, and (b−d) C 1s, Co 2p, and Se 3d high-resolution XPS spectra of u-CoSe@HCFs.

The surface composition and electronic status of u-CoSe@HCFs were studied by XPS spectra. As displayed in **Fig. S16**, the surface of the sample consists of C, N, Co, and Se elements. The C 1s high-resolution XPS spectrum of u-CoTe@HCFs (**Fig. S16b**) is deconvoluted into four peaks, which can be ascribed to C−C, C−N, C−O, and C=O bonds. The peak deconvolution of Co 2p high-resolution XPS spectrum shows that the peaks at 797.4 and 781.4 eV are related to Co $2p_{1/2}$ and Co $2p_{3/2}$, respectively (**Fig. S16c**). It is worth noting that the presence of the mixed oxidation states of the surface is related to the inevitable surface oxidation. Furthermore, The Se 3d high-resolution XPS spectrum in **Figure S16d** demonstrates that the spectrum can be mainly fitted into two peaks, including Se^{2-} $3d_{3/2}$ and Se^{2-} $3d_{5/2}$.[1]

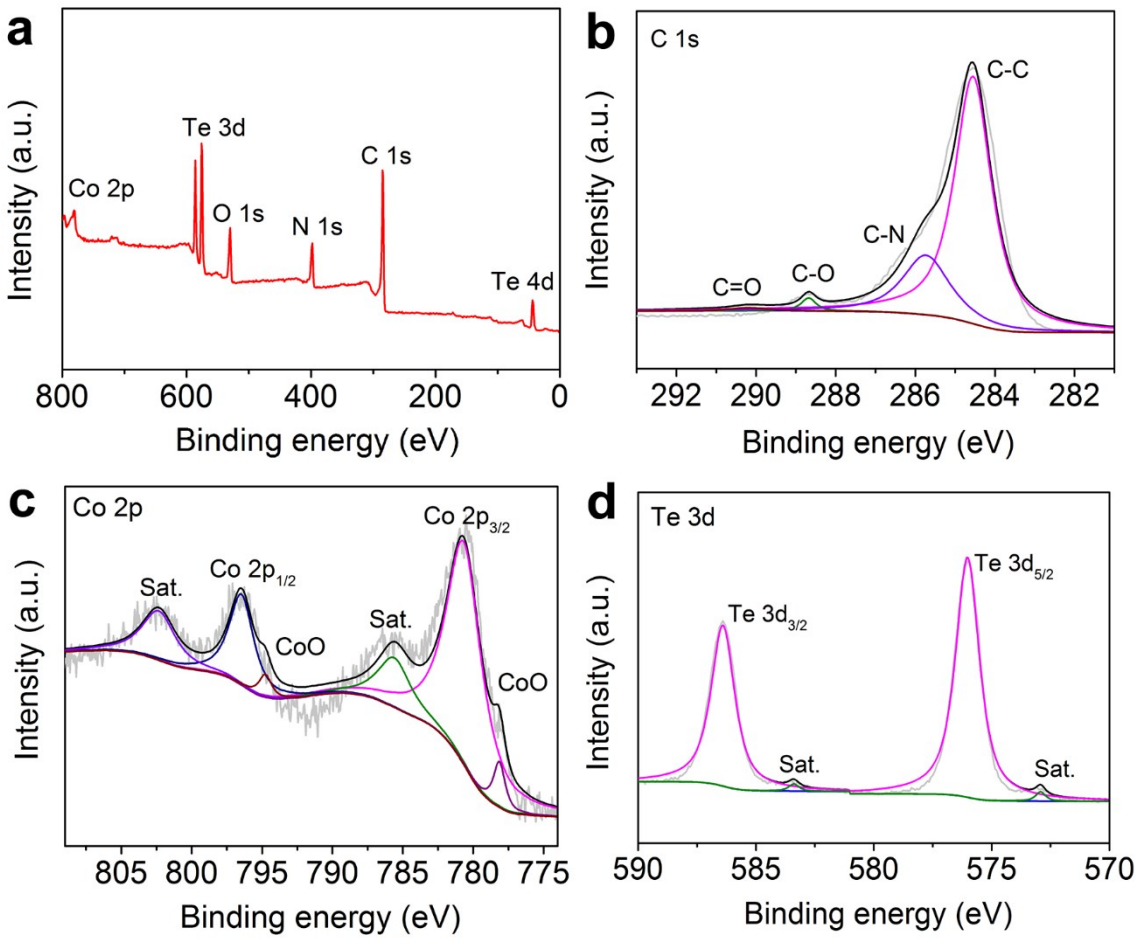

Fig. S17 (a) XPS survey scan, and (b−d) C 1s, Co 2p, and Te 3d high-resolution XPS spectra of u-CoTe@HCFs.

As shown in **Fig. S17**, the surface of the sample is composed of C, N, Co, and Te elements. The C 1s high-resolution XPS spectrum of u-CoTe@HCFs (**Fig. S17b**) is deconvoluted into four peaks, corresponding to C−C, C−N, C−O, and C=O bonds. The peak deconvolution of Co 2p high-resolution XPS spectrum illustrates that the peaks at 796.5 and 781.2 eV can be assigned to Co $2p_{1/2}$ and Co $2p_{3/2}$, respectively (**Fig. S17c**). It should be noted that the existence of the mixed oxidation states of the surface is due to the inevitable surface oxidation. In addition, The Te 3d high-resolution XPS spectrum in **Figure S17d** shows that the spectrum can be mainly fitted into two peaks, including Te^{2-} $3d_{3/2}$ and Te^{2-} $3d_{5/2}$.[2]

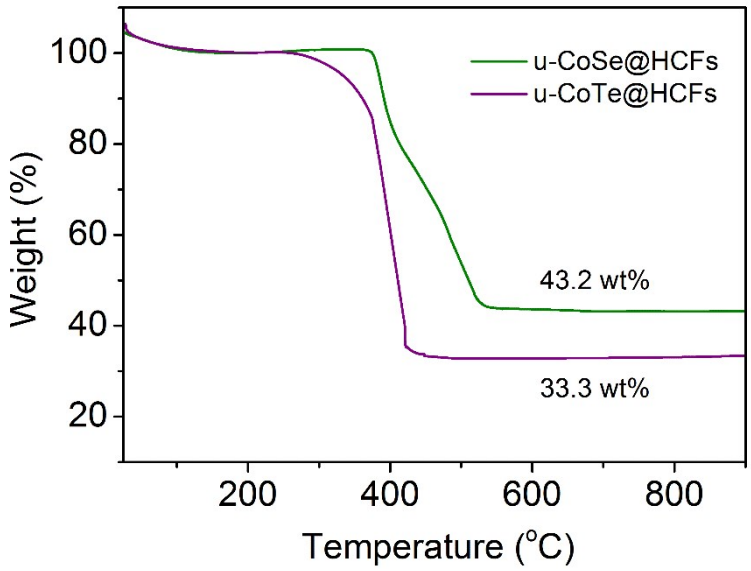

Fig. S18 TGA profiles of u-CoSe@HCFs and u-CoTe@HCFs under an air atmosphere with a heating rate of 10 °C min^{-1} from room temperature to 900 °C.

The respective weight percentage of CoSe and CoTe in u-CoSe@HCFs and u-CoTe@HCFs can be determined by TGA on the basis of the complete weight loss of HCFs combustion and the partial weight loss from the conversion of CoSe and CoTe to Co_3O_4. For example, the calculation formular of CoSe content is listed as follows. As a result, the content of CoSe and CoTe in u-CoSe@HCFs and u-CoTe@HCFs is calculated to be approximately 68 wt% and 73 wt%, respectively.

$$\text{CoSe (wt\%)} = \frac{\text{final weight of u-CoSe@HCFs}}{\text{initial weight of u-CoSe@HCFs}} \times \frac{3 \times \text{molecular weight of CoSe}}{\text{molecular weight of } Co_3O_4}$$

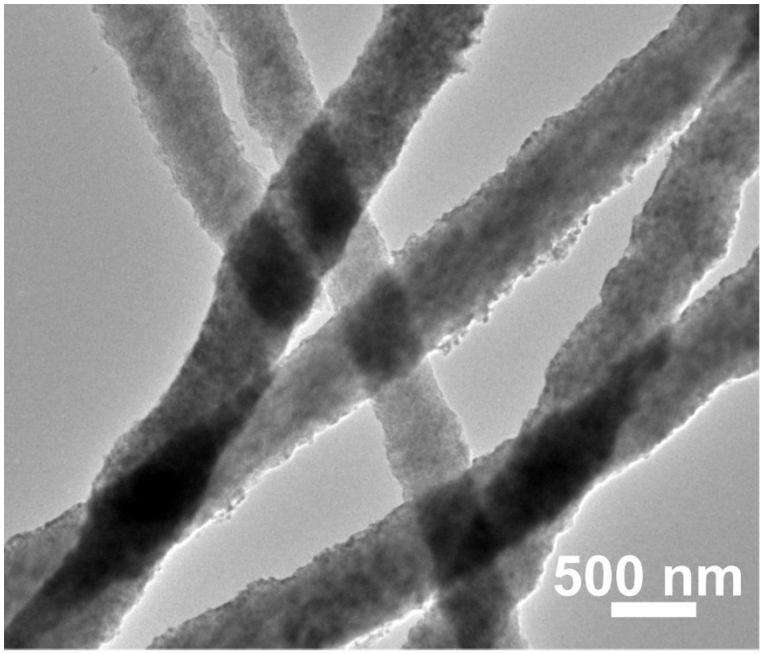

Fig. S19 TEM image of u-CoS_2@HCFs after intense ultrasonic treatment for 24 h.

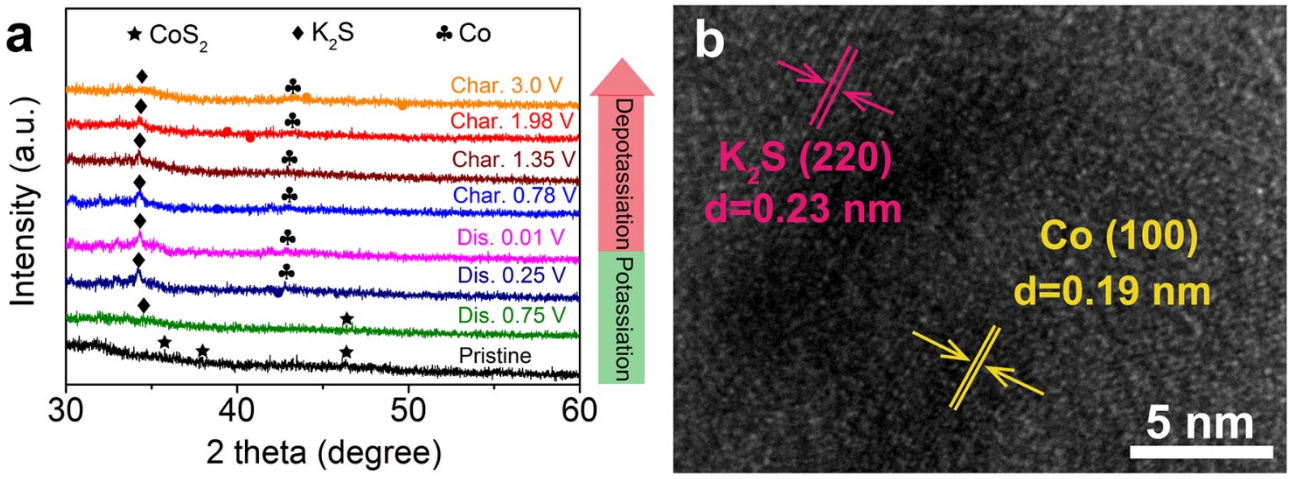

Fig. S20 (a) Ex situ XRD patterns of u-CoS_2@HCFs at various discharging/charging states and (b) HRTEM image of u-CoS_2@HCFs when first discharged to 0.01 V.

Remarkably, the peaks belonging to CoS_2 gradually disappear, while the peak belonging to K_2S and Co progressively increases during potassiation, indicating that the conversion reaction occurs between u-CoS_2@HCFs and K^+ ions. Furthermore, during the depotassiation process, the peak of K_2S and Co gradually weakens, indicating that the conversion reaction is reversible.

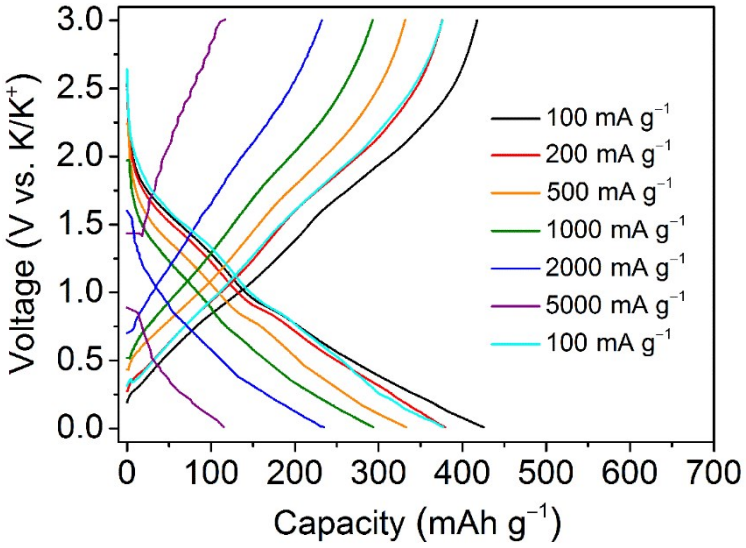

Fig. S21 Galvanostatic charge−discharge profiles of the u-CoS_2@HCFs electrode at various current densities.

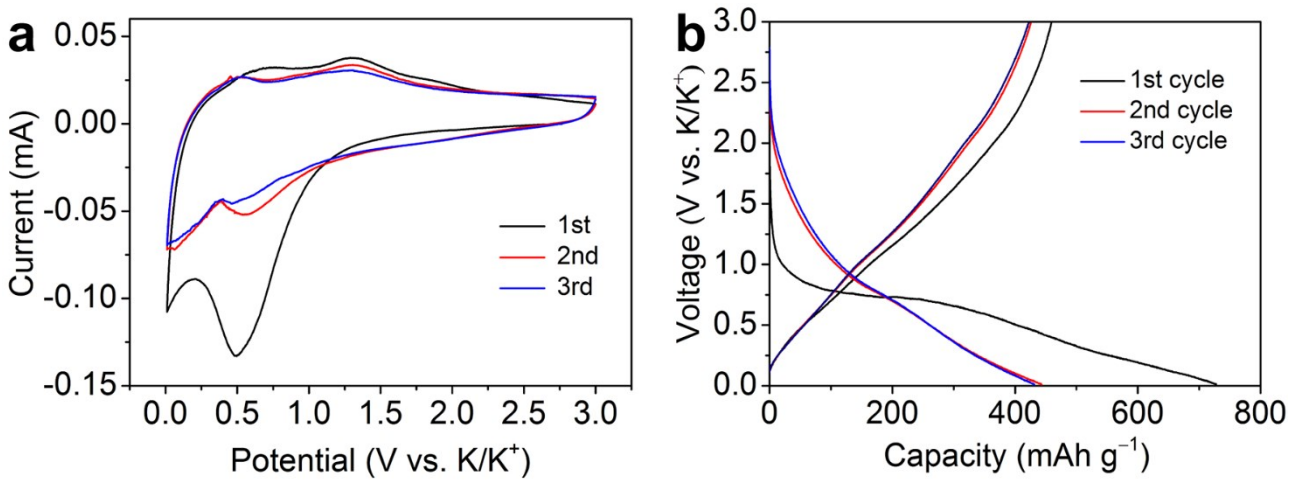

Fig. S22 Potassium storage properties of u-Co_3O_4@HCFs: (a) CV profiles at a sweep rate of 0.1 mV s^{-1} and (b) galvanostatic charge−discharge profiles of the initial three cycles at a current density of 100 mA g^{-1}.

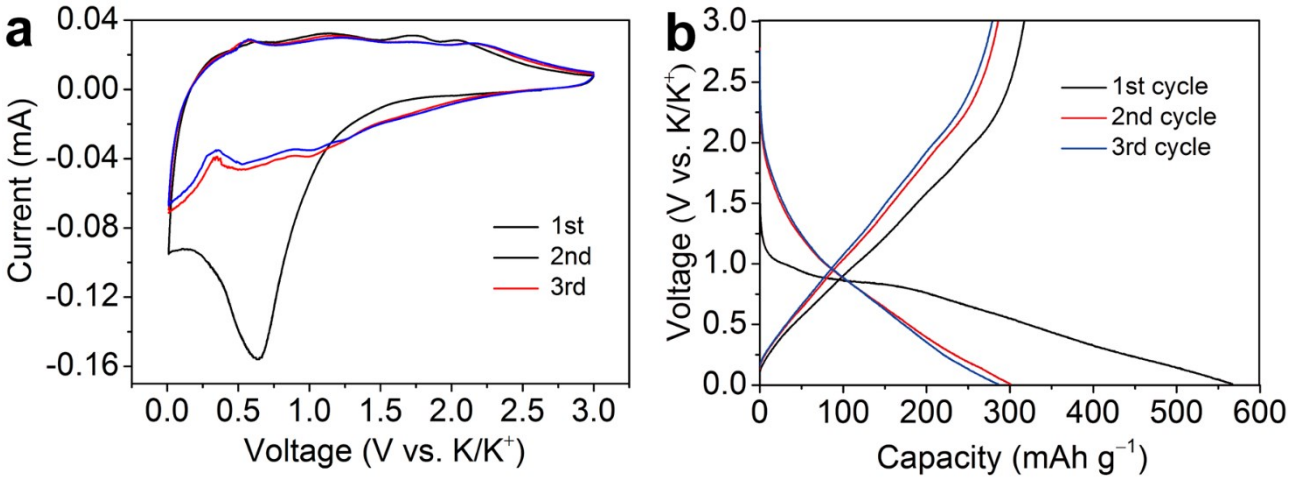

Fig. S23 Potassium storage performance of u-CoSe@HCFs: (a) CV curves at 0.1 mV s^{-1} and (b) galvanostatic charge−discharge profiles of the initial three cycles at 100 mA g^{-1}.

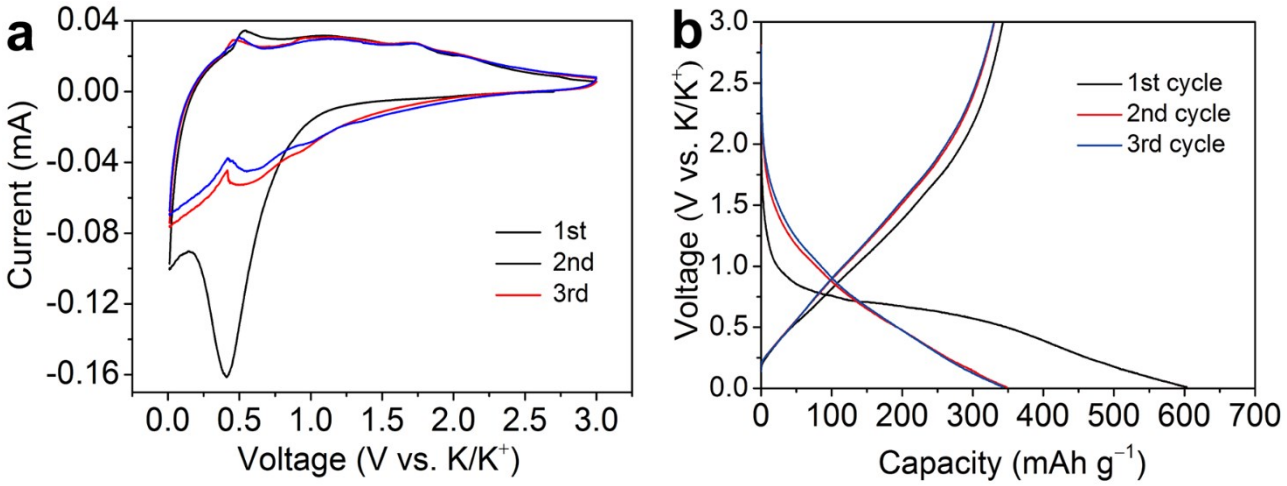

Fig. S24 Potassium storage properties of u-CoTe@HCFs: (a) CV profiles at 0.1 mV s^{-1} and (b) galvanostatic charge−discharge curves of the first three cycles at 100 mA g^{-1}.

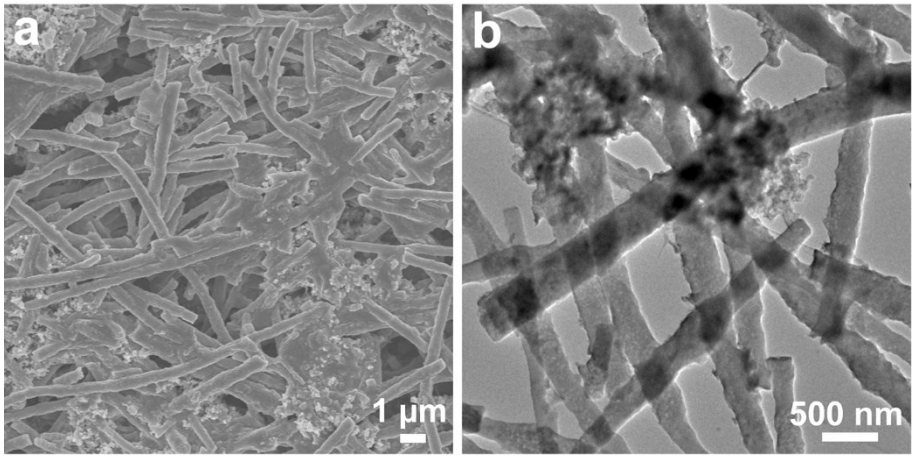

Fig. S25 (a) SEM images and (b) TEM images of u-Co_3O_4@HCFs after 500 charge−discharge cycles at 500 mA g^{-1}.

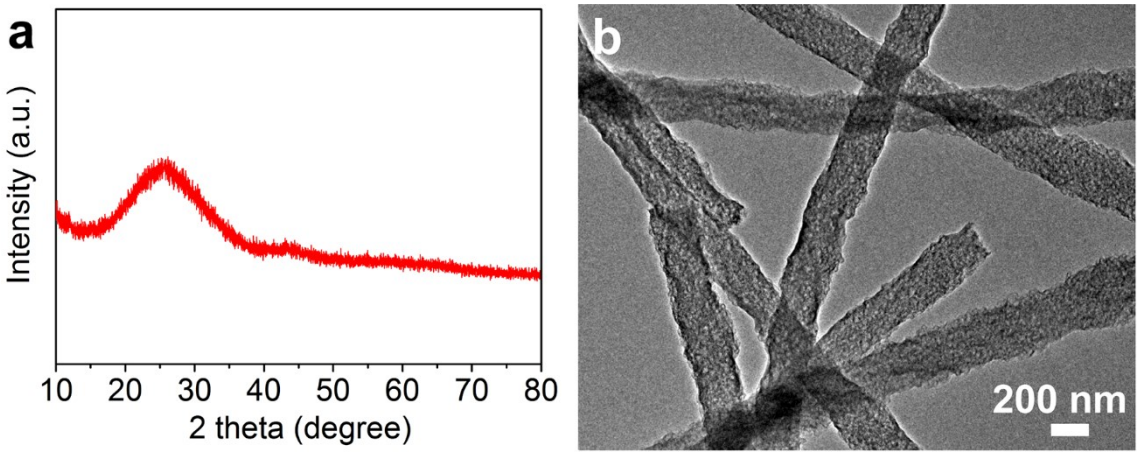

Fig. S26 (a) XRD pattern and (b) TEM image of HCFs.

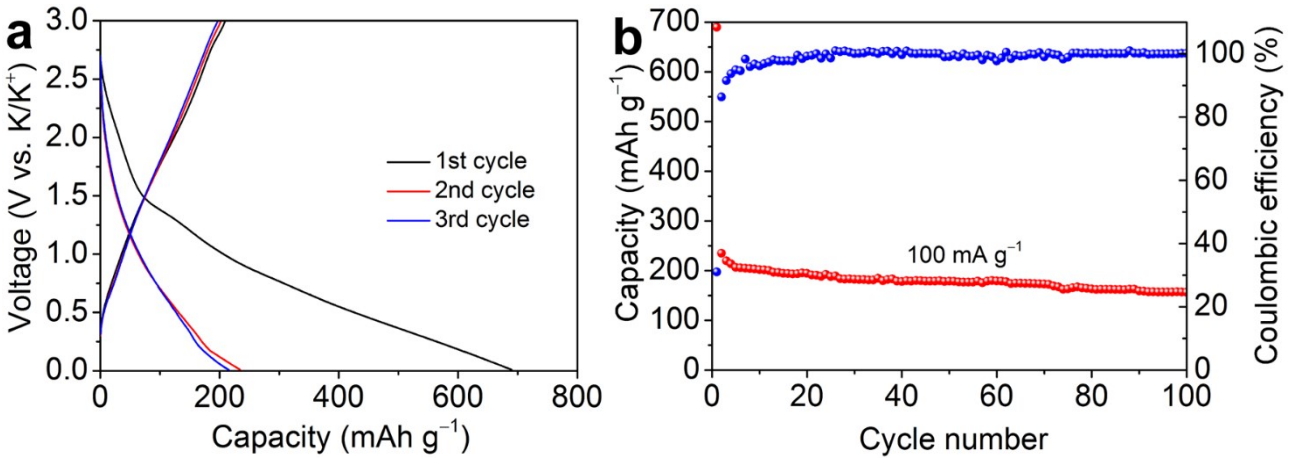

Fig. S27 Potassium storage properties of HCFs: (a) galvanostatic charge−discharge curves of the initial three cycles at 100 mA g^{-1} and (b) cycling performance.

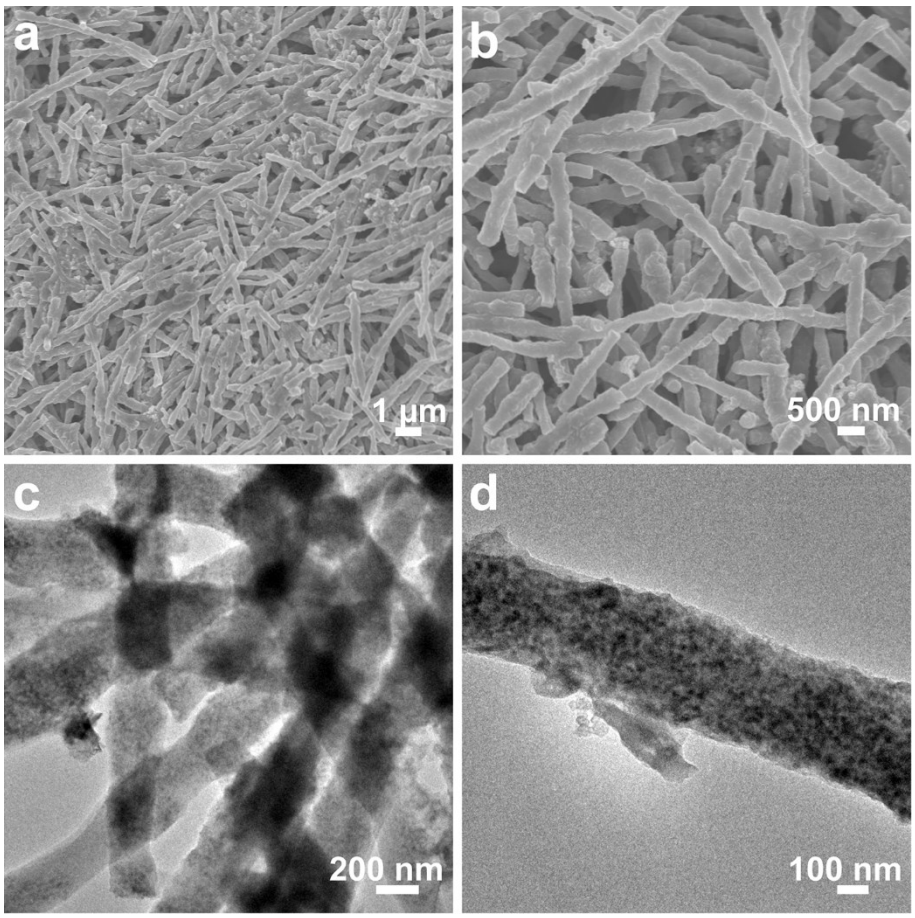

Fig. S28 (a, b) SEM images and (c, d) TEM images of u-CoS_2@HCFs after 1000 charge−discharge cycles at 500 mA g^{-1}.

Table S1. Control experiments for the preparation of different Co nanoparticles-embedded in hierarchically porous carbon nanofibers.

Sample	ZIF-67 (g)	PAN (g)	Final structure
LD-Co@HCFs	0.4	0.7	Low-density Co ultrasmall nanoparticles
u-Co@HCFs	0.5	0.7	High-density Co ultrasmall nanoparticles
LS-Co@HCFs	0.6	0.7	Large-size Co nanoparticles

Table S2. Micropore, mesopore, macroporous, and total volumes of various u-CoM_x@HCFs nanocomposites.

Sample	u-CoS_2@HCFs	u-Co_3O_4@HCFs	u-CoSe@HCFs	u-CoTe@HCFs
Micropore volume ($cm^3\ g^{-1}$)	0.031	0.022	0.019	0.017
Mesopore volume ($cm^3\ g^{-1}$)	0.056	0.046	0.043	0.038
Macropore volume ($cm^3\ g^{-1}$)	0.175	0.158	0.153	0.150
Total volume ($cm^3\ g^{-1}$)	0.262	0.226	0.215	0.205

Table S3. Comparison of potassium storage properties of u-CoS_2@HCFs and other anode materials.

Anode materials	Initial reversible capacity (mAh g^{-1})	Cycling property (mAh g^{-1})	Rate capability (mAh g^{-1})	Reference
u-CoS_2@HCFs	**330 (500 mA g^{-1})**	**269 (1000 cycles)**	**290 (1 A g^{-1})**	**This work**
AC@CoS/NCNTs/CoS@CNFs	182 (3.2 A g^{-1})	130 (600 cycles)	225 (0.8 A g^{-1})	3
CoS@G-25	435 (500 mA g^{-1})	310 (100 cycles) [a]	220 (4 A g^{-1})	4
Co_3O_4@N-C	235 (500 mA g^{-1})	213 (750 cycles)	169 (1 A g^{-1})	5
N/O doped carbon	315 (50 mA g^{-1})	231 (100 cycles)	160 (1 A g^{-1})	6
Ta_2NiSe_5	353 (50 mA g^{-1})	315 (50 cycles)	121 (1 A g^{-1})	7
MoS_2/N-doped-C	380 (100 mA g^{-1})	210 (100 cycles)	171 (0.5 A g^{-1})	8
Co_3O_4-Fe_2O_3/C	360 (50 mA g^{-1})	220 (50 cycles)	275 (1 A g^{-1})	9
MoS_2@SnO_2@C	600 (1 A g^{-1})	230 (450 cycles)	260 (1 A g^{-1})	10
FLNG [b]	352 (500 mA g^{-1})	150 (500 cycles)	170 (0.5 A g^{-1})	11
S@rGO sponges	400 (50 mA g^{-1})	361 (50 cycles)	225 (1 A g^{-1})	12
Sn_4P_3/C	355 (50 mA g^{-1})	307 (50 cycles)	260 (0.5 A g^{-1})	13
NPC [c]	190 (500 mA g^{-1})	121(1000 cycles)	210 (0.5 A g^{-1})	14
Hollow MoS_2/C microspheres	399 (20 mA g^{-1})	278 (20 cycles)	Not reported	15
$K_{0.6}Mn_1F_{2.7}$ hollow nanocubes	160 (50 mA g^{-1})	138 (100 cycles)	78 (1 A g^{-1})	16

[a] Note that the 100-cycle capacity retention of CoS@G-25 is 71.3%, which is much lower than the 1000-cycle capacity retention of u-CoS_2@HCFs (81.5%).

[b] FLNG: few-layer nitrogen-doped graphene.

[c] NPC: N-doped hierarchically porous carbon.

References

1. Q. Yu, B. Jiang, J. Hu, C.-Y. Lao, Y. Gao, P. Li, Z. Liu, G. Suo, D. He, W. A. Wang and G. Yin, *Adv. Sci.*, 2018, **5**, 1800782.
2. Y. Ding, W. Wang, M. Bi, J. Guo and Z. Fang, *Electrochim. Acta*, 2019, **313**, 331−340.
3. W. Miao, Y. Zhang, H. Li, Z. Zhang, L. Li, Z. Yu and W. Zhang, *J. Mater. Chem. A.*, 2019, **7**, 5504−5512.
4. H. Gao, T. Zhou, Y. Zheng, Q. Zhang, Y. Liu, J. Chen, H. Liu and Z. Guo, *Adv. Funct. Mater.*, 2017, **27**, 1702634.
5. D. Adekoya, H. Chen, H. Y. Hoh, T. Gould, M. S. J. T. Balogun, C. Lai, H. Zhao and S. Zhang, *ACS Nano*, 2020, **14**, 5027−5035.
6. J. Yang, Z. Ju, Y. Jiang, Z. Xing, B. Xi, J. Feng and S. Xiong, *Adv. Mater.*, 2018, **30**, 1700104.
7. H. Tian, X. Yu, H. Shao, L. Dong, Y. Chen, X. Fang, C. Wang, W. Han and G. Wang, *Adv. Energy Mater.*, 2019, **9**, 1901560.
8. B. Jia, Q. Yu, Y. Zhao, M. Qin, W. Wang, Z. Liu, C.-Y. Lao, Y. Liu, H. Wu, Z. Zhang and X. Qu, *Adv. Funct. Mater.*, 2018, **28**, 1803409.
9. I. Sultana, M. M. Rahman, S. Mateti, V. G. Ahmadabadi, A. M. Glushenkov and Y. Chen, *Nanoscale*, 2017, **9**, 3646−3654.
10. Z. Chen, D. Yin and M. Zhang, *Small*, 2018, **14**, 1703818.
11. Z. Ju, P. Li, G. Ma, Z. Xing, Q. Zhuang and Y. Qian, *Energy Storage Mater.*, 2018, **11**, 38−46.
12. J. Li, W. Qin, J. Xie, H. Lei, Y. Zhu, W. Huang, X. Xu, Z. Zhao and W. Mai, *Nano Energy*, 2018, **53**, 415−424.
13. W. Zhang, J. Mao, S. Li, Z. Chen and Z. Guo, *J. Am. Chem. Soc.*, 2017, **139**, 3316−3319.
14. X. Qi, K. Huang, X. Wu, W. Zhao, H. Wang, Q. Zhuang and Z. Ju, *Carbon*, 2018, **131**, 79−85.
15. T. Yang, J. Liang, I. Sultana, M. M. Rahman, M. J. Monteiro, Y. Chen, Z. Shao, S. R. P. Silva and J. Liu, *J. Mater. Chem. A.*, 2018, **6**, 8280−8288.
16. Z. Liu, P. Li, G. Suo, S. Gong, W. Wang, C.-Y. Lao, Y. Xie, H. Guo, Q. Yu, W. Zhao, K. Han, Q. Wang, M. Qin, K. Xi and X. Qu, *Energy Environ. Sci.*, 2018, **11**, 3033−3042.